Few-Body Systems 10, 105–133 (1991)

Few-Body Systems

Deuteron Photodisintegration at Low Energies*

K.-M. Schmitt, P. Wilhelm, and H. Arenhövel

Institut für Kernphysik, Johannes-Gutenberg-Universität, J.-J.-Becher-Weg 45, D-W-6500 Mainz, Federal Republic of Germany

Abstract. All presently available experimental data on deuteron photodisintegration below 40 MeV (i.e., total and differential cross sections, photon asymmetry and neutron polarization) are collected and carefully compared with the present status of the conventional theory (i.e., in the framework of meson-theoretical or semi-phenomenological N-N potentials including subnuclear degrees of freedom and relativistic corrections). No significant evidence for a failure of the conventional theory is found within the present experimental accuracy.

1 Introduction

Deuteron disintegration has a long history in nuclear physics, and the role of the deuteron as a test case for theoretical concepts of the N-N interaction and of subnuclear degrees of freedom in electromagnetic processes is well established [1]. The reason for this special role is that the deuteron "is the simplest of all nuclear systems and its properties are as important in nuclear theory as the hydrogen atom is in atomic theory" [2]. Recently, the emphasis has shifted towards the role of quark-gluon degrees of freedom of QCD in nuclei and, therefore, the important question arises: Is there any experimental evidence for a failure of the conventional framework of nuclear theory using nucleon, meson and isobar degrees of freedom only in the electromagnetic break-up of the deuteron at low energy, which belongs to the non-perturbative regime of QCD? To answer this question, two requirements have to be met: First, on the theoretical side one has to ascertain to have made every effort for a consistent conventional description. And secondly, on the experimental side, a sufficiently high accuracy is required for being able to detect any significant disagreement with the results of the conventional calculation.

By choosing deuteron photodisintegration at low energies as the object of our investigations, the first condition is met for several reasons: If the energy region is sufficiently restricted—to below 40 MeV, say—uncertainties concerning relativistic corrections and isobar configurations as well are strongly suppressed. Furthermore, gauge independence of nonrelativistic calculations is fulfilled to a very high degree. Therefore, the theoretical results are almost uniquely fixed, once the N-N potential

* Partially supported by the Deutsche Forschungsgemeinschaft (SFB 201)

is given. Finally, in view of the high degree of sophistication of present theoretical concepts of N-N potentials it is timely to make a detailed and as complete as possible comparison with experiments. Thus, our basic motivation is twofold: First, we want to summarize the current status of the conventional theory in comparison with the experimental data and secondly, we hope that these investigations will stimulate further experimental studies on this process.

The organization of the paper is as follows: In Sect. 2 we define our theoretical input. We use as meson-theoretical potentials the various OBE approximations to the recent Bonn potential and the Paris potential. Besides consistent static meson-exchange currents (MEC), we also include isobar configurations (IC), the relativistic spin-orbit current and in one case lowest-order retardation currents. In Sect. 3 we compare our results with all available experimental data for the total cross section and in Sect. 4 with differential cross sections. In Sect. 5 we discuss the few polarization observables already measured in this energy region, namely, the photon asymmetry and the neutron polarization. Finally, a summary is given in Sect. 6. Already here we would like to apologize for possible oversights of existing data.

2 Theoretical Ingredients

Concerning the N-N interaction we use potentials which represent the presently most reliable conventional approaches, namely the meson-theoretical Bonn potential [3] and the dispersion-theoretical Paris potential [4]. But for convenience we substitute in both cases the full potential models by their corresponding semi-phenomenological one-boson-exchange (OBE) approximations. Thus, in the case of the Bonn potential, we consider the relativistic OBEPQ, the energy-dependent OBEPT, and the nonrelativistic OBEPR as given in ref. [3]. The energy-independent OBEPs have been criticized by Desplanques [5] because of their low D-state admixture P_D and their poor ε_1 mixing parameter. In a model study, he demonstrated that P_D should be increased by 1.5–2 percent if a phase-equivalent static potential is derived from a corresponding energy-dependent one. This criticism has been partially taken into account in the new versions of the OBEPQ and OBEPR as given in Tables A.1 and A.3 of ref. [6], respectively. Note that two of the OBEPQ models lead to a similarly good description of the experimental ε_1 like the Bonn full model or the Paris potential [7]. Already here we would like to remark that the potential-model dependence concerning the different versions of the Bonn potential is not significant in the energy range and for the observables discussed here in view of the experimental uncertainties.

Concerning the electromagnetic interaction we include

— static meson-exchange currents (MEC) consistent with the potential model,
— isobar currents (IC) and
— relativistic corrections (RC).

The MEC contributions are partially included via the Siegert operators in the so-called normal part (N), which includes also the nonrelativistic one-body current. The remainder is treated as explicit MEC, where only π- and ρ-contributions are taken into account. Whereas this decomposition is, of course, gauge-dependent, since the choice of a special form of the Siegert operators means nothing else but choosing a special electromagnetic gauge, the sum of N and explicit $(\pi + \rho)$-MEC

is only negligibly gauge-dependent as discussed in detail in ref. [8]. This fact strongly supports the consistency of the incorporated MEC contributions. To achieve this balance, it is necessary to carefully incorporate the strong form factors of the given potential into the explicit π- and ρ-MEC, as discussed in ref. [9], since these form factors give rise to additional regularization currents. In case of the energy-dependent OBEPT, we also include lowest-order retardation currents for the π and ρ, which stem from the non-instantaneous meson propagation. The construction of these currents is guidelined by the formalism given in ref. [10], and the application to the OBEPT is discussed in ref. [9]. The problem of slight non-orthogonality of the wave functions for the OBEPT due to its explicit energy dependence is neglected, since it has been shown in ref. [10] that the dominant contribution appears to come from current retardation.

The IC contributions are implemented following ref. [11]. The isobar configurations are treated in impulse approximation, which is sufficient in the energy region considered here.

The RC are dominated by the two-body part [12] of the relativistic spin-orbit (SO) current [13]. But we take into account also its one-body part. In case of the OBEPs we include furthermore lowest-order relativistic corrections to the one-body current [10] beyond the SO current.

For the calculation of observables we use the standard multipole decomposition of the reaction T-matrix including electric and magnetic multipoles up to the order $L = 4$, if not stated otherwise.

3 The Total Cross Section

Modern experimental techniques allow the determination of the total cross section for deuteron photodisintegration with an accuracy distinctly below the 5 percent level. Within the energy region considered, the reaction is sensitive to electric and magnetic dipole contributions only as evident in Fig. 1 for the case of the OBEPR.

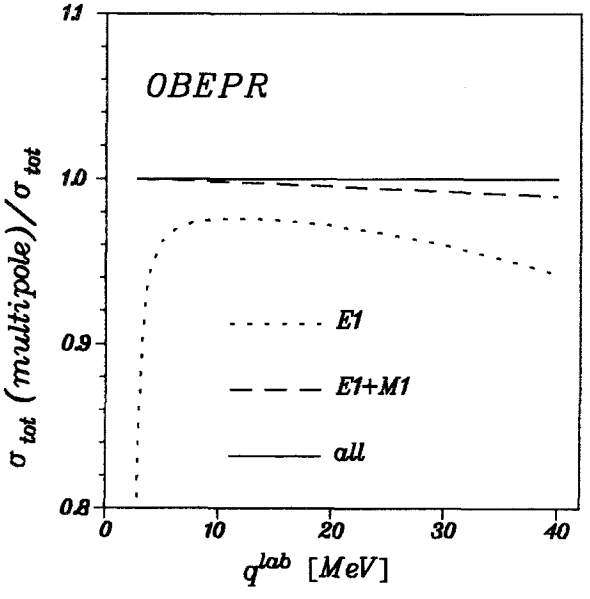

Fig. 1. Relative multipole contributions to the total cross section for the OBEPR. The reference value σ_{tot} includes electric and magnetic multipoles up to $L = 4$

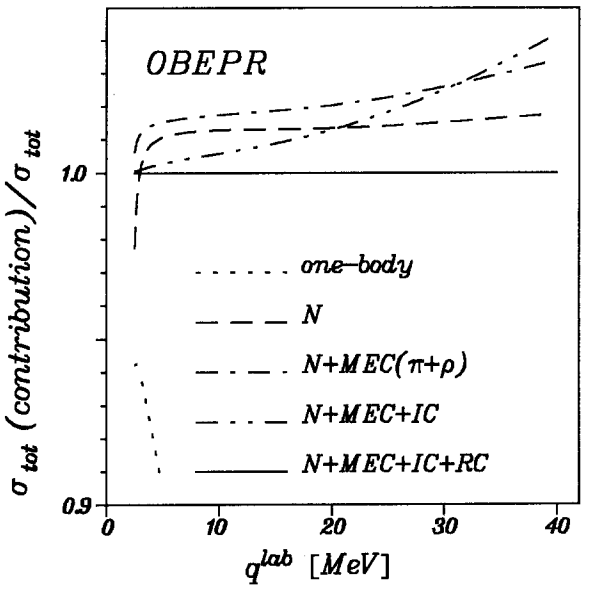

Fig. 2. Relative contributions to the total cross section for the OBEPR from the various electromagnetic currents. "one-body" denotes the pure nonrelativistic convection and spin current, i.e., without use of any Siegert operators

In view of the fact that the various electromagnetic current contributions show up significantly on the few-percent level, as is demonstrated in Fig. 2 again for the OBEPR, we would like to emphasize that high-precision measurements of the total cross section on the order of one percent are quite important. For the other potentials the situation is quite similar.

For the following comparison with experimental data we normalize for convenience all theoretical and experimental cross sections to the classical effective-range (ER) cross section [14]

$$\sigma_{\mathrm{ER}} = \sigma_{\mathrm{ER}}(\mathrm{E1}) + \sigma_{\mathrm{ER}}(\mathrm{M1}). \tag{1}$$

The electric dipole part including finite-size effects is given by

$$\sigma_{\mathrm{ER}}(\mathrm{E1}) = \frac{8\pi}{3}\frac{\alpha}{\kappa^2}\frac{(\gamma-1)^{3/2}}{\gamma^3(1-\kappa r_t)}, \tag{2}$$

where α denotes the fine-structure constant, $\kappa = \sqrt{ME_B}$, with M the nucleon mass and E_B the deuteron binding energy, r_t is the triplet effective range and $\gamma = q/E_B$, with q the incident photon energy. The magnetic dipole contribution is given in this simple model by

$$\sigma_{\mathrm{ER}}(\mathrm{M1}) = \frac{2\pi}{3}\frac{\alpha}{M^2}(\mu_p-\mu_n)^2\frac{k\kappa}{k^2+\kappa^2}\frac{\left(1-\kappa a_s+\frac{a_s}{4}(r_s+r_t)\kappa^2-\frac{a_s}{4}(r_s-r_t)k^2\right)^2}{(1+k^2a_s^2)(1-\kappa r_t)} \tag{3}$$

with proton (μ_p) and neutron (μ_n) magnetic moments, the singlet effective range r_s, the singlet scattering length a_s, and the asymptotic proton-neutron relative momentum k.

Table 1 contains in column 2 the references of total cross section measurements below 40 MeV since 1950. In columns 3 and 4 the energy range and the corresponding accuracy of the measurements are indicated. Without going into experimental

Table 1. Experiments on total cross section for deuteron photodisintegration in the energy range $q^{lab} \leqslant 40$ MeV and χ^2-probabilities of theoretical results using various potential models and for the effective-range cross section

				$P(\chi^2)$					
				Bonn OBEP-					
No.	Ref.	q^{lab}/MeV	Accuracy [percent]	Q	T	R	Paris	ER	
1	[15]	20–40	1–2	1.00	1.00	1.00	1.00	1.00	χ
2	[16]	2.75	3	0.35	0.15	0.21	0.42	0.63	
3	[17]	⩾15	5–7	0.47	0.97	0.24	0.02	0.31	
4	[18]	6–11	1–6	0.72	0.90	0.58	1.00	1.00	
5	[19]	14.7	6	0.95	0.97	0.92	0.86	0.75	
6	[20]	⩾10	3–4	0.04	0.49	0.27	0.94	1.00	
7	[21]	⩾21	4–8	0.36	0.67	0.43	0.81	1.00	
8	[22]	15–25	2–4	0.26	0.87	0.03	0.41	0.97	
9	[23]	17–28	5–7	0.23	0.86	0.12	0.29	0.95	
10	[24]	17–27	6	1.00	1.00	1.00	1.00	1.00	χ
11	[25]	5–10	10–35	0.85	0.87	0.84	0.82	0.81	E
12	[26]	⩾27	6–7	0.99	0.99	1.00	1.00	1.00	χ
13	[27]	9.43	6	0.65	0.72	0.60	0.46	0.33	
14	[28]	9.43	20	0.09	0.13	0.07	0.02	0.03	E
15	[29]	9–23	12–21	0.05	0.03	0.08	0.20	0.40	E
16	[30]	⩾23	9–10	0.56	0.14	0.72	0.92	0.99	
17	[31]	2.75	3	0.43	0.58	0.54	0.37	0.14	
18	[32]	2.62	2	0.97	1.00	0.98	0.98	0.89	χ
19	[33]	4–18	5–12	0.05	0.10	0.04	0.03	0.03	E
20	[34]	15–18	21–23	0.02	0.04	0.01	0.00	0.02	E
21	[35]	2.5–2.8	4–7	1.00	1.00	1.00	1.00	0.99	χ
22	[36]	17.6	21	0.18	0.26	0.13	0.06	0.03	E
23	[37]	6.55	14	0.84	0.85	0.84	0.82	0.80	E
24	[38]	2.76	8	0.38	0.31	0.33	0.41	0.50	
25	[70]	15	3	0.72	0.89	0.50	0.05	0.44	

details for each of the measurements, it should be mentioned that these experiments are based on a wide range of different methods: radiative decay of excited nuclear states provided the photon beam in experiments nos. 2, 4, 17–24. A continuous bremsstrahlung beam was used in nos. 8, 10, 12, 15, and 16 and a monochromatic beam in no. 3. Some of the experiments (nos. 12 and 16) measured the differential cross section, from which the total cross section was deduced. The experiments nos. 1, 5, 7, 13, 14, and 70 measured the inverse process of radiative neutron capture by protons and used the principle of detailed balance. Finally, the equivalent photon cross section was extracted from a deuteron electrodisintegration measurement in no. 9.

To have a rough but quantitative measure of the degree of agreement or disagreement of the experimental results with the theoretical predictions, we calculate the corresponding χ^2-probabilities: For N given experimental values e_i with errors σ_i and corresponding theoretical results t_i we define

$$\chi^2 = \sum_{i=1}^{N} \frac{(t_i - e_i)^2}{\sigma_i^2} \tag{4}$$

and, assuming Gaussian distributions for each measurement, the probability of finding deviations less than χ^2 is given by

$$P(\chi^2) = \int_0^{\chi^2} d\chi'^2 \, P_N(\chi'^2) \tag{5}$$

with the χ^2-distribution

$$P_N(\chi^2) = \frac{1}{2^{N/2}\Gamma(N/2)} \chi^{N-2} e^{-\chi^2/2}. \tag{6}$$

Of course, the assumption of pure Gaussian errors is somehow questionable, since not all of the references in Table 1 do give separately the statistical errors. But due to the large data base of Table 1 there is nevertheless some hope that with the help of χ^2 we will be able to exclude experiments with large inherent but unknown systematic errors.

The χ^2-probabilities $P(\chi^2)$ are listed in columns 5–9 of Table 1 for the OBEPQ, -T, -R, the Paris potential and for the effective-range theory of Eq. (1), respectively. In order to select a clean data base from Table 1, which is to be used in a proper comparison with the theory, we first neglect all experiments which include measurements with given errors larger than 10 percent. This concerns nos. 11, 14, 15, 19, 20, 22, and 23 and is indicated by an "E" in column 10. Secondly, we exclude all experiments with $P(\chi^2) > 95$ percent for all models OBEPQ, -T, -R and the Paris potential. This concerns nos. 1, 10, 12, 18, and 21 and is denoted by a "χ" in column 10. Further justification for excluding these experiments is provided by a closer look at their results: nos. 10 and 21 are without any doubt incompatible with other experiments in the same energy regions. Nos. 1 and 18 give very likely too small errors, and no. 12 is ruled out by its 30 MeV result, which is at variance with the general trend of experimental data and which, furthermore, lies 3–5 standard deviations below any realistic theory. Thus, we are left with those experiments of Table 1 without any label in column 10. Finally, the experiments nos. 2, 17, and 24 are substituted by their weighted mean values.

Only this reduced data base is now compared to the theory in Figs. 3 a and 3 b. The corresponding χ^2-probabilities are listed in Table 2. Taking all experiments from the reduced data base together (see row "a + b" of Table 2), neither the OBEPT, which gives cross sections too low, nor the Paris potential results, which lie too high, are compatible with the experimental cross sections. On the other hand, OBEPQ and -R results are in agreement with the experimental data, but the corresponding $P(\chi^2)$ seems to indicate an overestimation of error bars. The situation becomes clearer, if one takes the experiments from groups "a" and "b" from Table 2 and Fig. 3 separately: The more recent data of group "a" experiments provide an ideal $P(\chi^2)$ for OBEPQ and -R, whereas -T and the Paris potential show significant

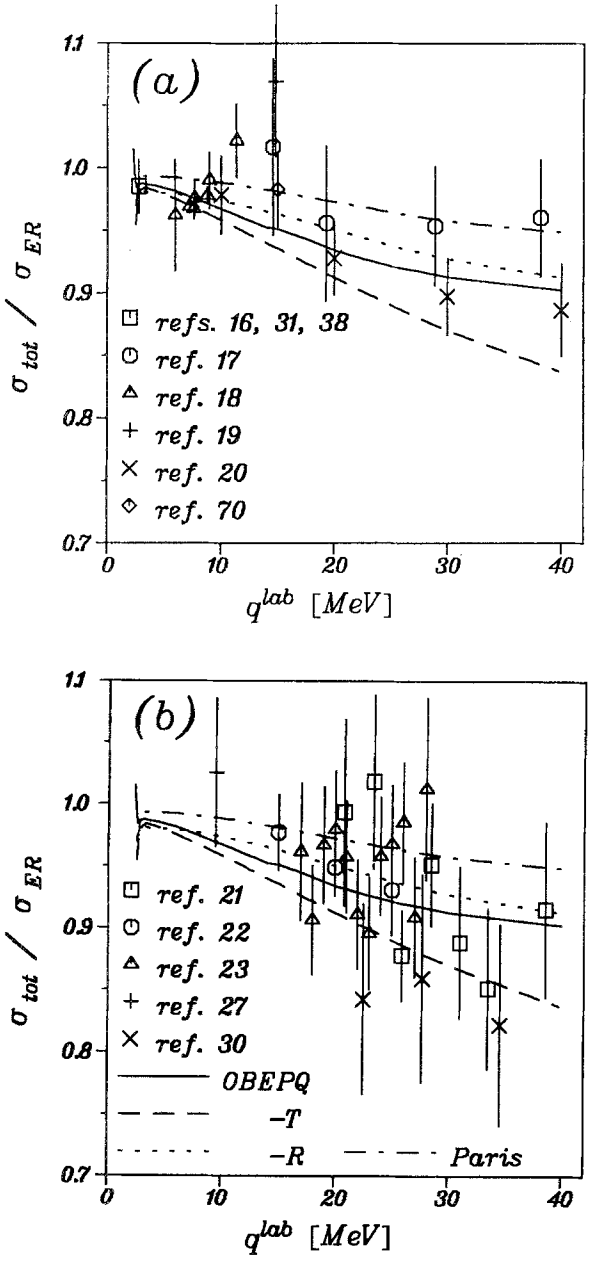

Fig. 3. Theoretical and experimental total cross sections normalized to the effective-range theory. Only the reduced data base of Table 1 is included divided into two groups "a" and "b" according to Table 2

deviations. The older data for group "b" include large experimental errors and, thus, are much less sensitive. Note that the ER theory is significantly ruled out by the data.

It is also worth mentioning that the variation of the total cross section with the different OBEPQ versions lies below two percent and thus the corresponding χ^2-probabilities are close to each other. The same is true for the different OBEPR models.

Coming back to the different current contributions to the total cross section shown in Fig. 2, it is mandatory, in view of the present experimental accuracy, to include IC and RC contributions even in the low-energy region. This can be seen by comparing the different curves of Fig. 2 with the reduced data base of Table 1:

Table 2. χ^2-probabilities $P(\chi^2)$ for different theoretical models with respect to the reduced data base of Table 1. "a" denotes the experiments nos. 2–6, 17, 24 and 70 and "b" denotes nos. 7–9, 13 and 16

	$P(\chi^2)$				
	OBEP				
	-Q	-T	-R	Paris	ER
a	0.51	0.99	0.31	1.00	1.00
b	0.13	0.84	0.09	0.64	1.00
a + b	0.19	0.99	0.08	0.99	1.00

In case of the OBEPR, including only N + MEC(π + ρ) yields a $P(\chi^2) = 0.99$. But further inclusion of IC or of IC + RC reduces $P(\chi^2)$ to 0.55 or 0.08, respectively.

4 The Differential Cross Section

As we have shown in the previous section, the conventional theory of deuteron photodisintegration is compatible with the experimental total cross section data in the energy region from threshold up to 40 MeV. Whether this is also true for the differential cross section will be discussed in this section.

Contrary to the total cross section, angular distributions depend coherently on the different multipole transitions. Therefore, measurements of the differential cross section provide in principle information not only on the moduli of the electromagnetic matrix elements but also on their phases. To illustrate the interference of the different multipoles we show in Fig. 4 the differential cross section at 20 MeV for the case of the OBEPR as it is obtained by successively adding multipole contributions of increasing order.

One readily notes the overwhelming dominance of E1 due to transitions to $^3P_0$, $^3P_1$, $^3P_2$, and $^3F_2$ partial waves while the $^1P_1$ spin-flip transition is suppressed by two orders of magnitude. This pure E1-part of the cross section has the typical (a + b $\sin^2 \Theta_p^{cm}$)-shape. Formally, this can be seen by first expanding the differential cross section in terms of Legendre polynomials,

$$\frac{d\sigma}{d\Omega} = \sum_l a_l P_l(\cos \Theta_p^{cm}). \tag{7}$$

Explicit expressions for the coefficients a_l in terms of the various multipole matrix elements are given in refs. [71] and [72]. These expressions contain angular-momentum and parity-selection rules limiting the possible multipole interference terms. Then it follows from parity conservation that the even (odd) Legendre coefficients a_l include only multipole interference terms with the same (opposite) parity. Furthermore, if the multipolarities of the matrix elements in question are denoted by L and L', the triangular angular-momentum inequalities for (l, L, L')

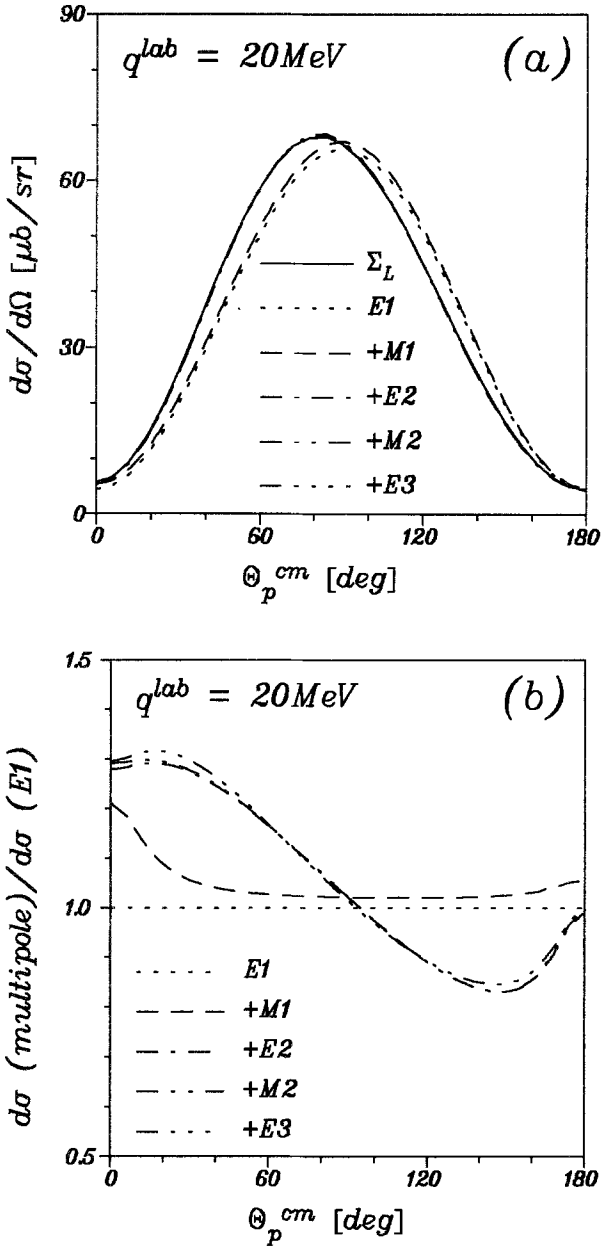

Fig. 4. Absolute (a) and relative (b) electromagnetic multipole contributions to the differential cross section at 20 MeV for the OBEPR. "E1" denotes the pure electric dipole content, whereas "+E2", for example, denotes the coherent contributions of E1, M1, and E2 multipoles. "Σ_L" includes all multipoles up to $L = 4$. Θ_p^{cm} denotes the angle between the outgoing proton and the incoming photon momentum in the cm system

have to be fulfilled. Thus, restricting Eq. (7) to E1 transitions, only a_0 and a_2 survive and one obtains the mentioned symmetric shape.

M1 transitions mainly lead to the $^1S_0$ and $^1D_2$ partial waves in the energy region considered, whereas the non-spin flip transitions to $^3S_1$, $^3D_1$, and $^3D_2$ are suppressed by an order of magnitude. Inclusion of E1 and M1 in Eq. (7) changes a_0 and a_2 through M1-M1 contributions and leads to a nonvanishing a_1 due to E1-M1 interferences. However, the symmetry around $\Theta_p^{cm} = 90°$ and the absolute size of the cross section are very little affected. Only at extreme forward and backward angles, where the cross section falls off rapidly, M1 contributions become important. We shall come back to this aspect later on.

The E2 operator gives the lowest non-negligible transitions to isospin $T = 0$ partial waves and, thus, the E2 matrix elements govern the asymmetry of the cross section via E1-E2 contributions to a_1 and a_3. It is noteworthy that all $T = 0$ partial waves are of comparable importance concerning this interference, and the asymmetry around 90° is essentially determined by the structure of the E2 operator. At 20 MeV photon energy higher multipoles beyond E2 are negligible for the differential cross section as is obvious from Fig. 4. But at higher energies they will become sizable, for instance in the forward cross section as discussed below.

Concerning the different electromagnetic currents, we show in Fig. 5 their contributions to the differential cross section at 20 MeV. Similarly to what was found

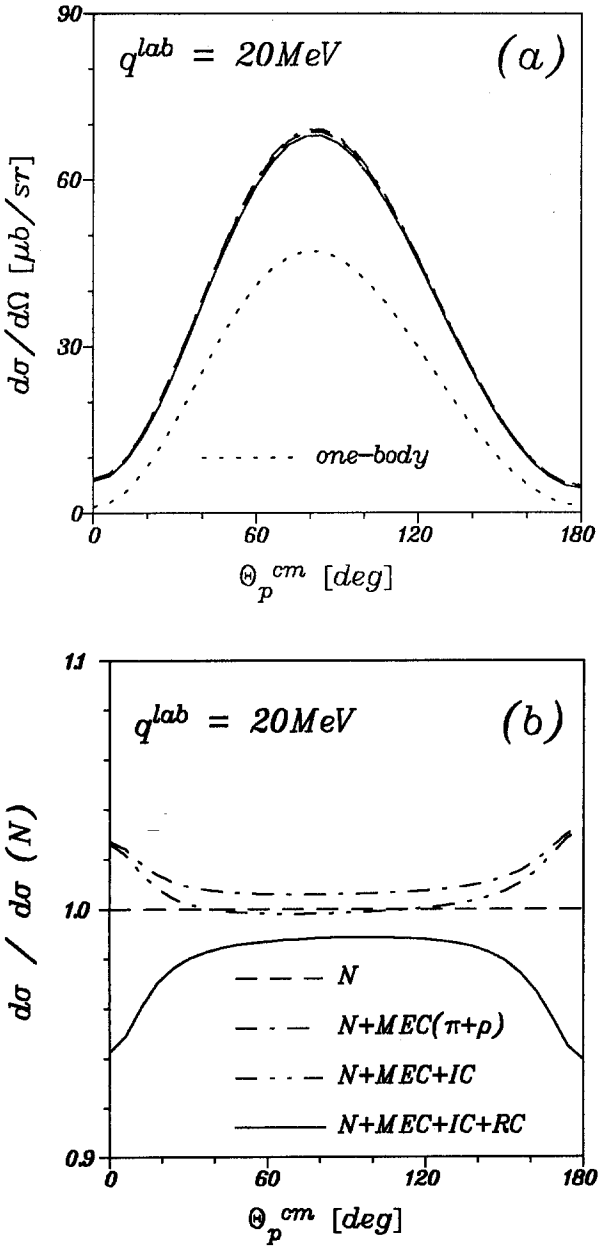

Fig. 5. The various current contributions to the differential cross section at 20 MeV for the OBEPR in absolute (a) and relative (b) representation

for the total cross section, it is given by the normal part on the few-percent level for intermediate angles. But at extreme forward and backward angles explicit MEC beyond the Siegert operator enhance the cross section, whereas the spin-orbit current reduces it considerably.

In order to investigate the energy dependence of the differential cross section we shall use the Legendre coefficients of Eq. (7) rather than the old-fashioned de Swart-Partovi coefficients [39, 40]. The coefficient a_0 being proportional to the total

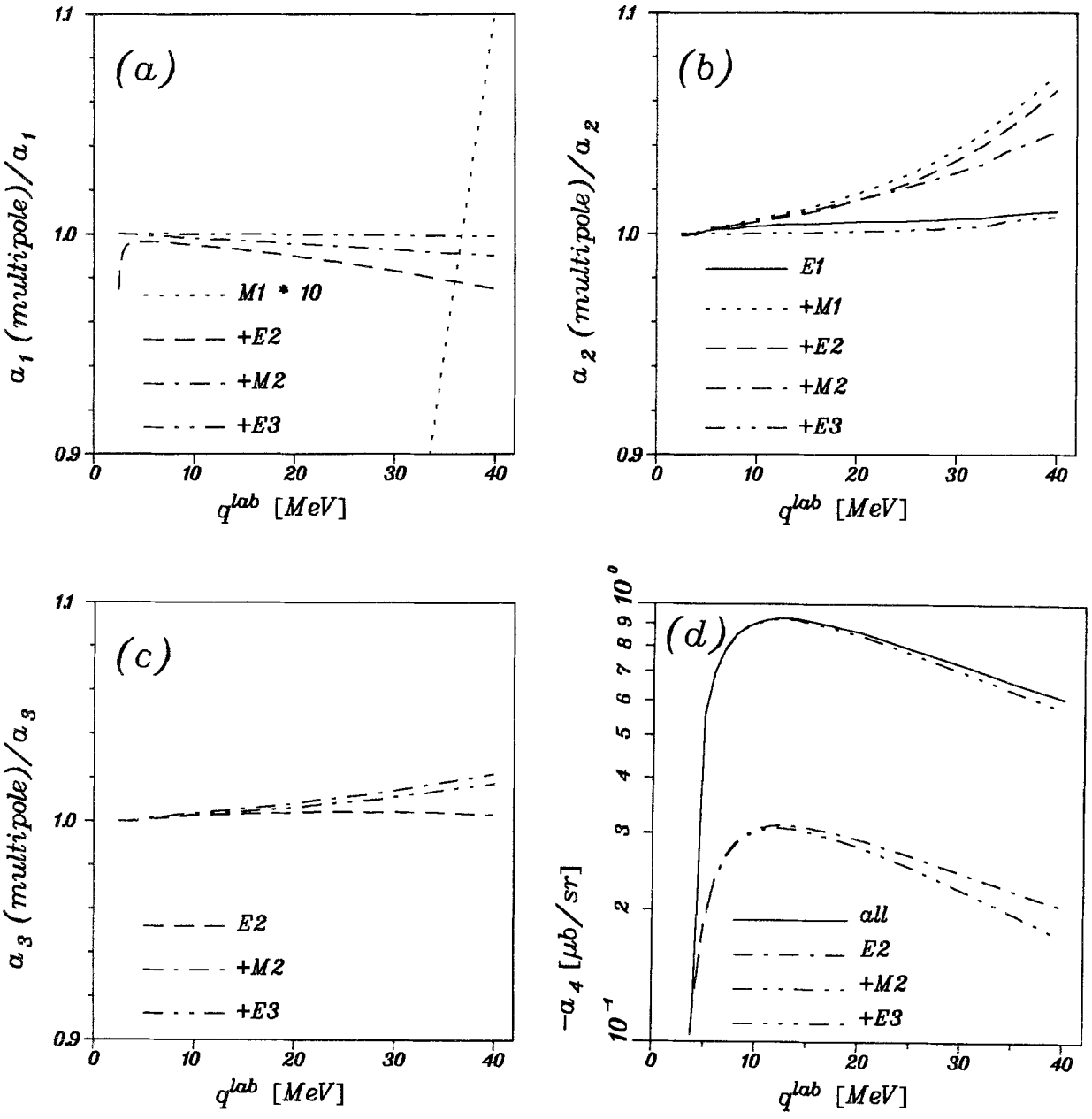

Fig. 6. Relative (a_1–a_3) and absolute (a_4) multipole contributions to Legendre coefficients for OBEPR as function of the photon energy with respect to the total result including all multipoles up to $L = 4$. The notation is explained in Table 3. Note that for a_1 the E1-M1 term is multiplied by a factor 10

cross section has been discussed already in the previous section. We show in Fig. 6 the remaining a_l ($l = 1$–4) with the different multipole contributions in the energy region considered. The various multipole interference terms which enter the corresponding a_l are listed in Table 3.

Except at threshold, the asymmetry of the angular distributions is dominantly given by "+ E2", i.e. by a pure E1-E2 interference in the case of a_3 and by an additional small E1-M1 contribution in the case of a_1. Only "+ M2", which essentially is due to M1-M2 interference, and "+ E3", a pure E2-E3 interference, contribute furthermore on the few percent level to a_1. The same is true for a_3, where now "+ E3" is dominantly given by E2-E3 interference, but a destructive interference with higher multipoles (mainly E1-E4) reduces a_3 to its E1-E2 part.

Surprisingly, it is the symmetric part of the differential cross section which is more sensitive to the multipole interferences as it becomes evident from the analysis of the a_2 coefficient. However, since there is a clear cancellation, mainly between M1-M1 and "+ E3", for which only the E1-E3 interference is relevant here, the pure E1-E1 part accidentally describes the total a_2 strength quite well. Concerning a_4 the dominant contributions come from E1-E3 and E2-E2 interferences, but a_4 is rather small on the absolute scale (see Fig. 9).

The relative contributions of the various electromagnetic currents to the lowest-order Legendre coefficients are shown in Fig. 7. It is interesting to see that including consistent MEC only (dash-dotted curves) the odd coefficients are almost constantly overestimated compared to the total result by about 2 percent in absolute size over

Table 3. Multipole interferences contributing to the lowest-order Legendre coefficients a_1 through a_4 including E1, M1, E2, M2, and E3. Column 2 defines the notation used in Fig. 6

a_l	Notation	Multipole interferences
a_1	M1	E1-M1
	+E2	+E1-E2
	+M2	+M1-M2 + E2-M2
	+E3	+E2-E3
a_2	E1	E1-E1
	+M1	+M1-M1
	+E2	+E2-M1 + E2-E2
	+M2	+E1-M2 + M2-M2
	+E3	+E1-E3 + E3-M2 + E3-E3
a_3	E2	E1-E2
	+M2	+M1-M2 + E2-M2
	+E3	+E3-M1 + E2-E3
a_4	E2	E2-E2
	+M2	+M2-M2
	+E3	+E1-E3 + E3-M2 + E3-E3

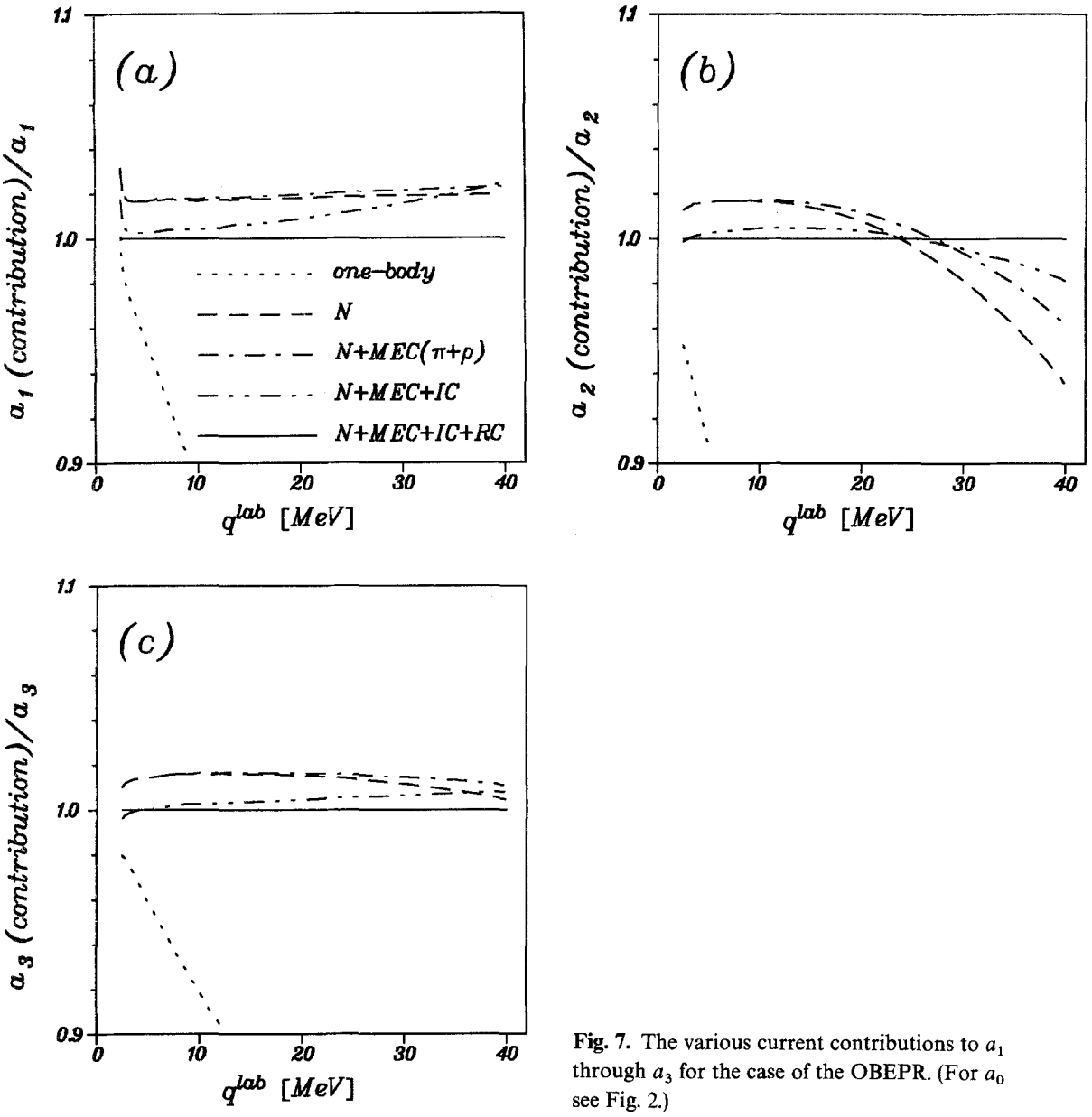

Fig. 7. The various current contributions to a_1 through a_3 for the case of the OBEPR. (For a_0 see Fig. 2.)

the whole energy range. Below 10 MeV the reduction is solely caused by IC contributions, whereas at higher energies the spin-orbit part of RC becomes important. The even coefficients show a different behaviour (for a_0 see Fig. 2). There the interplay of the interfering contributions is rather subtle, and all contributions beyond the normal part are non-negligible on the few percent scale.

A comparison of the results of the conventional theory with experimental data on the differential cross section is shown in Fig. 8, where we have included three experiments. Fink et al. [41] recently have measured the inverse radiative neutron-proton capture cross section for incoming neutron kinetic energies $T_n^{\text{cap}} = 19$–50 MeV, corresponding to equivalent photon laboratory energies of $q^{\text{lab}} = 12$–27 MeV for the disintegration process (the superscript "cap" denotes the laboratory system

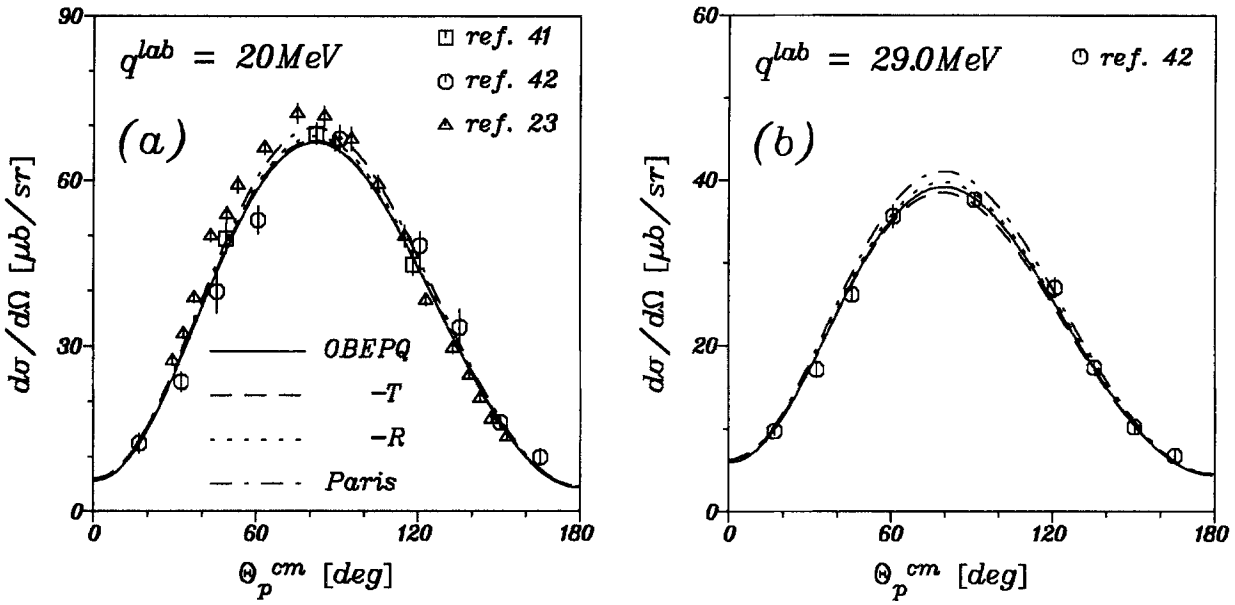

Fig. 8 a, b

Fig. 8. Comparison of different theoretical models with experimental angular distributions of the differential cross section from deuteron photodisintegration and neutron capture

of the capture process, where the initial proton is at rest). They also have analyzed the angular distributions in terms of Legendre coefficients, denoted by "a_l-fit" in Figs. 8 d and e. We have renormalized the data of ref. [41] to the total cross section of the OBEPR. This was necessary, since Fink et al. normalized to the absolute cross section measurements of ref. [24], which lie systematically below measurements reported by other authors. In Figs. 8 d and e the results of ref. [41] are shown for their lowest and highest T_n^{cap} value. In Fig. 8 a their data for $T_n^{cap} = 36$ MeV corresponding to $q^{lab} = 20.25$ MeV is compared with other experimental results at the same energy.

From De Pascale et al. [42] we have taken the data for $q^{lab} = 19.8$, 29.0, and 38.6 MeV, see Figs. 8 a–c, respectively. They used monochromatic photons produced by Compton back-scattering of laser light off high-energy electrons. Since they report cross section ratios only, we have renormalized the angular distributions to the theoretical total cross sections (OBEPQ). At 20 MeV there are also data available from Skopik et al. [23], who extracted the equivalent photon cross section from deuteron electrodisintegration measurements.

As is evident from Fig. 8, the comparison between experiment and theoretical calculations is much less conclusive than it was for the total cross section, and most likely this is due to systematic errors still present in these experiments. This suspicion is supported by the fact that, for example, at 20 MeV the different experimental results are significantly incompatible with each other, if the given errors are interpreted as statistical errors only, i.e., if they do not contain any systematic contribution. For instance, compared to the OBEPQ cross section the Fink data have a χ^2-probability of 0.37, but the data of De Pascale et al. and Skopik et al. yield both corresponding values > 0.99. The data for De Pascale et al. indicate a slight shift of the maximum towards larger proton angles, whereas the data of Skopik et al.

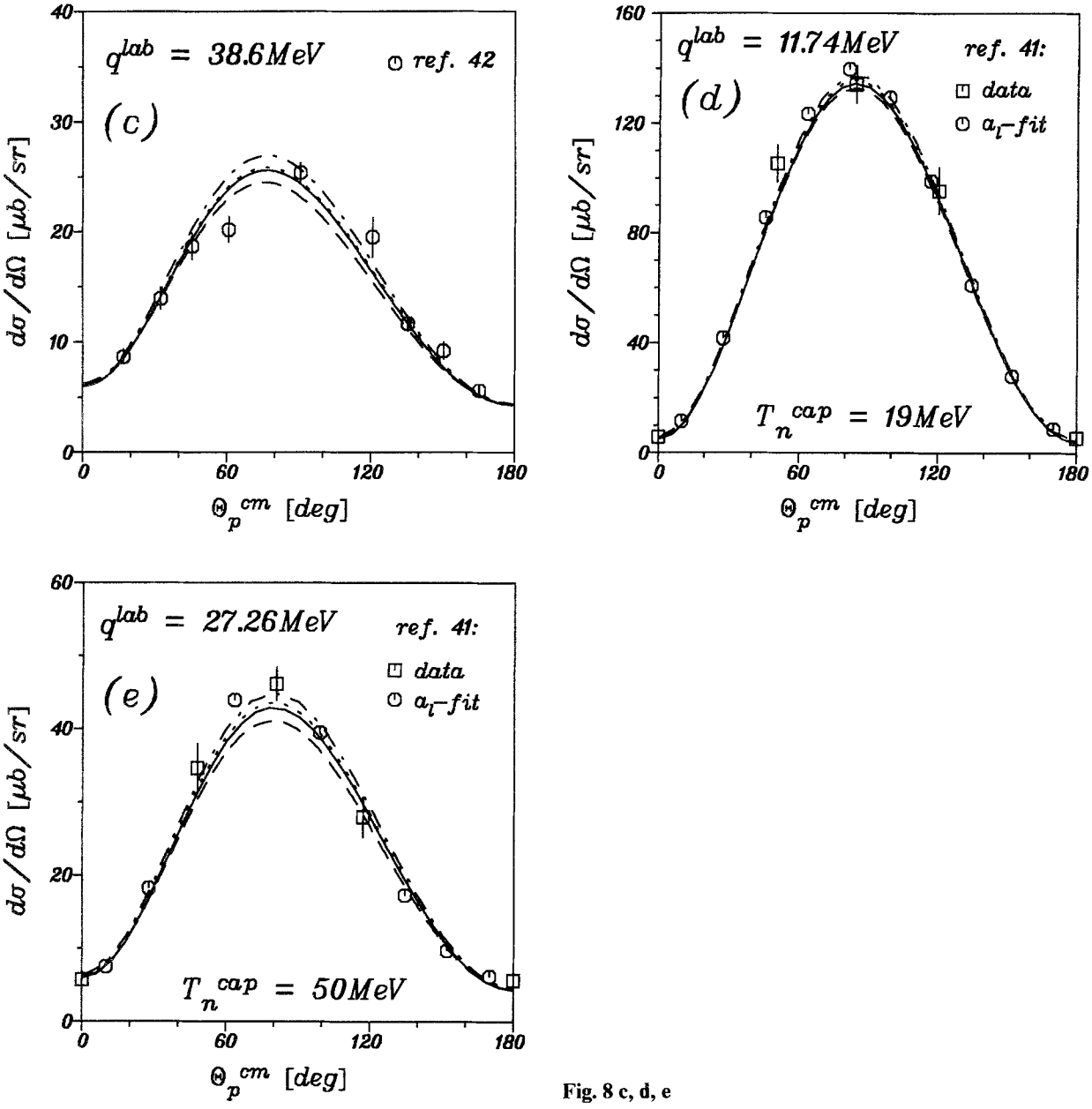

Fig. 8 c, d, e

indicate a shift towards smaller angles. Thus both are incompatible with each other and with the theory.

Comparing only the Fink data with the theory at the three energies considered in Fig. 8, one obtains acceptable χ^2-probabilities for all potential models OBEPQ, -T, -R and the Paris potential. On the other hand, the data by De Pascale et al. are statistically incompatible with all these models, except OBEPQ and -R at 29 MeV. However, taking into account the discrepancy to the data by Skopik et al. at 20 MeV, one neither can state an agreement nor a conclusive disagreement of the experimental data with theoretical predictions for the angular distributions, but rather faces an open situation in which more accurate data are required.

Besides definite angular distributions, there are also energy-dependent fits of the Legendre coefficients of the differential cross section available in the energy region considered. These were given by Fink et al. [41] at nine different energies within $19 \leqslant T_n^{\mathrm{cap}}/\mathrm{MeV} \leqslant 50$, at which energies they measured the angular distribution of the neutron capture process, and by De Pascale et al. [20], who analyzed world-wide data on deuteron photodisintegration and gave the a_l-coefficients in the energy region $10 \leqslant q^{\mathrm{lab}}/\mathrm{MeV} \leqslant 120$ in 10 MeV steps. Furthermore, two bidimensional fits

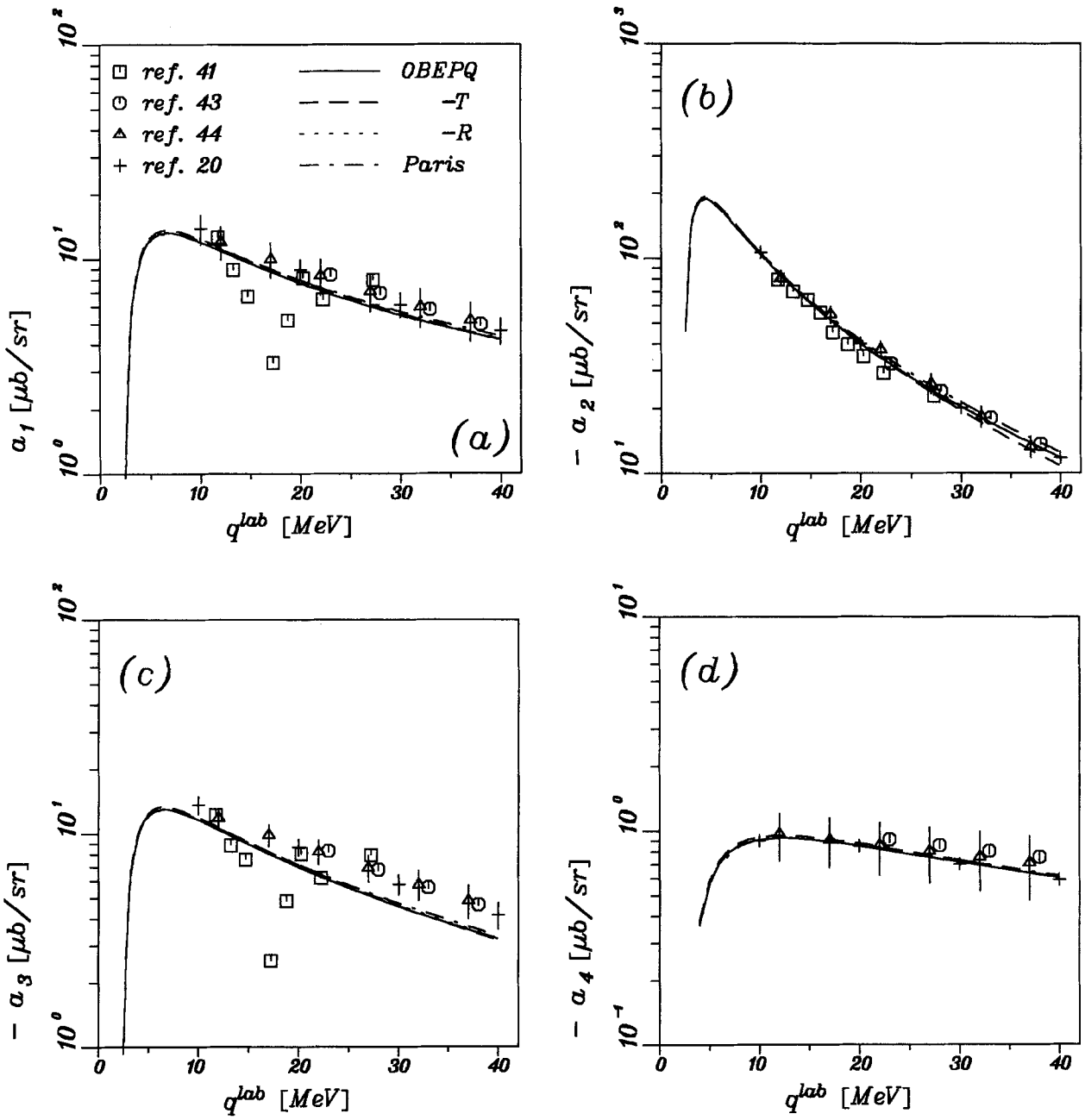

Fig. 9. Results of various experimental fits to the differential cross section in terms of Legendre polynomials in comparison with theoretical calculations

have been reported. One of them was given by Rossi et al. [43] for the energy region $20 \leqslant q^{\text{lab}}/\text{MeV} \leqslant 440$ and the other by Thorlacius and Fearing [44] for $10 \leqslant q^{\text{lab}}/\text{MeV} \leqslant 625$. Both fits use the same phenomenological energy dependence of the a_l-coefficients. However, using different data bases, they obtained extremely different errors. The relative uncertainties for the a_l-coefficients of Rossi et al. are smaller by an order of magnitude than those of Thorlacius and Fearing. However, one should keep in mind that these bidimensional fits serve for qualitative purposes only but not for a quantitative comparison as has been pointed out in ref. [1].

The results of these fits in comparison with theoretical calculations are shown in Fig. 9. One first notes an untypical behaviour of the odd Fink coefficients between

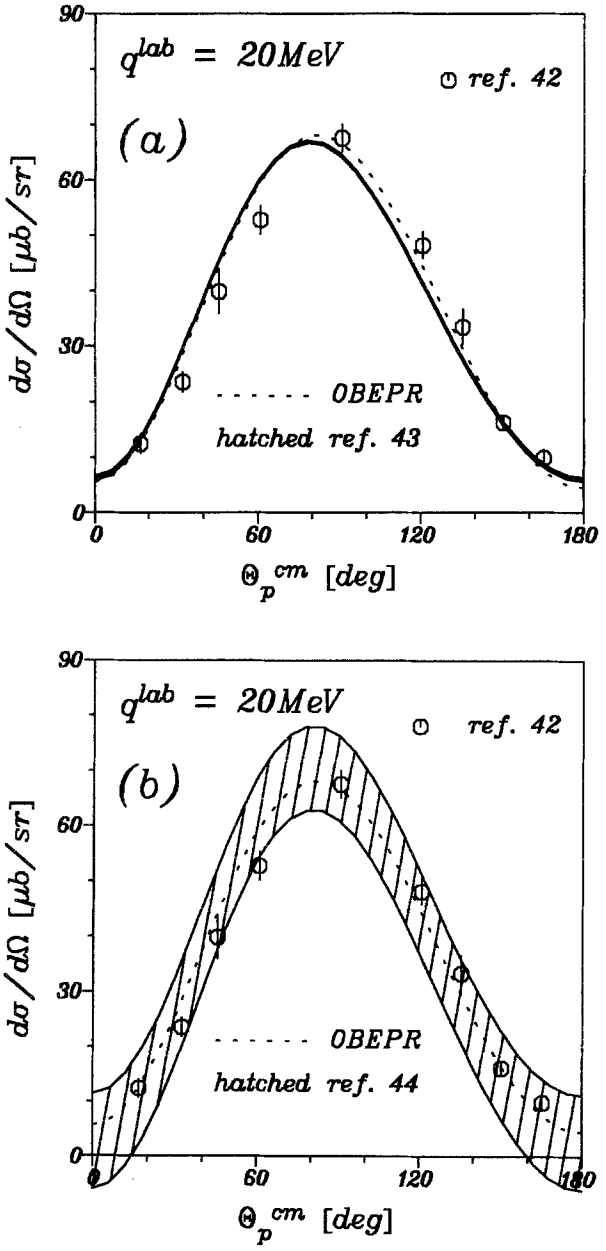

Fig. 10. Angular distribution at 20 MeV based on the Rossi (a) and Thorlacius (b) fits of a_l-coefficients including the statistical uncertainties in comparison with the measurement of ref. [42] and the calculation for the OBEPR

10 and 20 MeV. This indicates a systematic error in connection with the unfolding procedure of neutron capture events and $^{12}C(n, n'\gamma)^{12}C$ events, which were detected simultaneously. Therefore, also the angular distributions of ref. [41] are problematic for these energies. With respect to the bidimensional fits, the errors of Thorlacius and Fearing seem to be too pessimistic. On the other hand, there is a strong indication that the errors of the fit by Rossi et al. are considerably underestimated, since the corresponding angular distribution is incompatible with both the theory and the explicit measurement of ref. [42] (see Fig. 10). This underlines the above remark that one should be cautioned against comparisons based on these fits with theoretical calculations. At most, these fits should be considered qualitatively as helpful tools for quickly getting rough estimations.

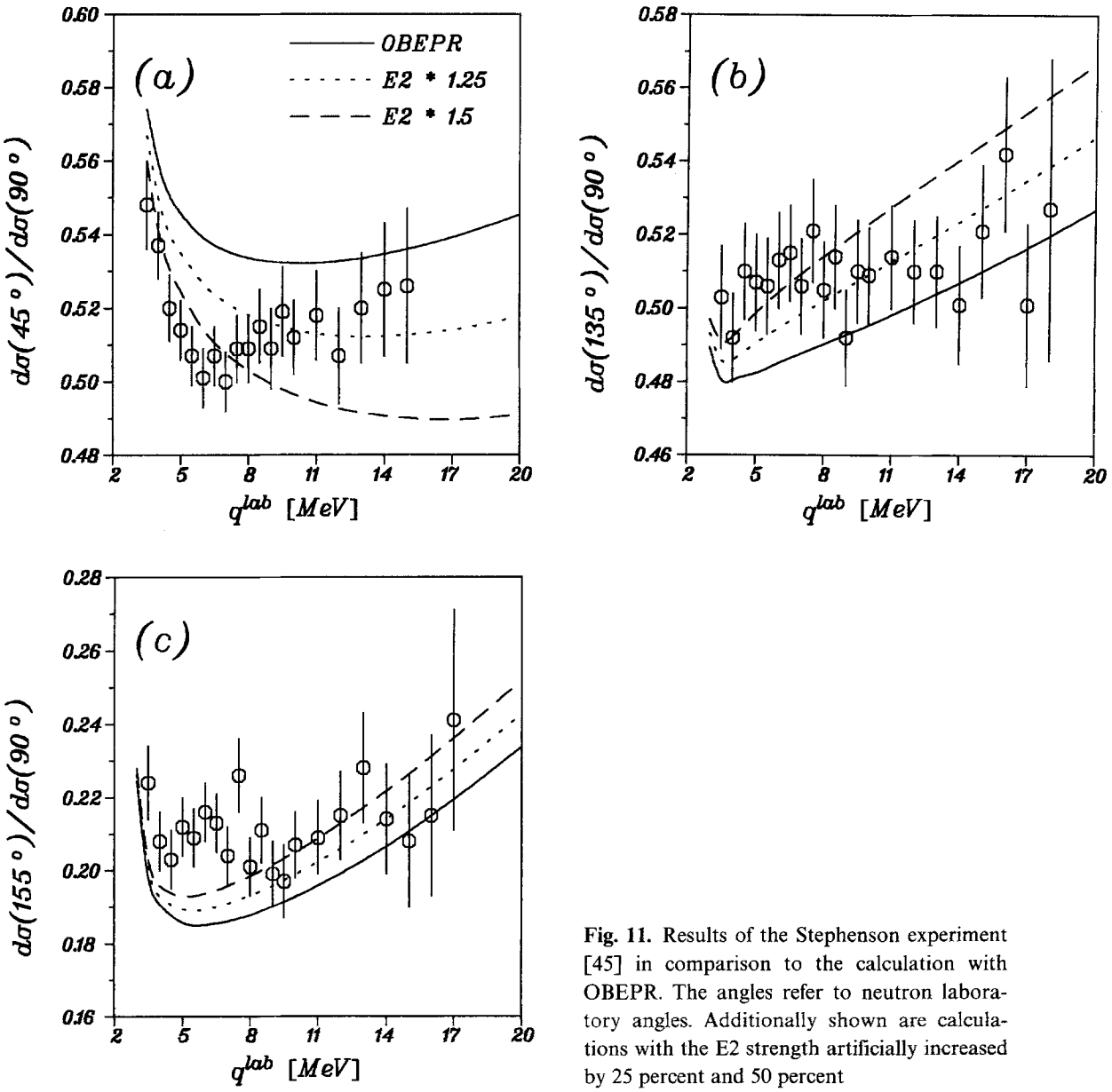

Fig. 11. Results of the Stephenson experiment [45] in comparison to the calculation with OBEPR. The angles refer to neutron laboratory angles. Additionally shown are calculations with the E2 strength artificially increased by 25 percent and 50 percent

Because of its rather large errors, the fit of De Pascale et al. is compatible with theoretical results for a_1. However, all experimental fits indicate for a_1 and a_3 a systematic deviation towards higher absolute values over the whole energy range from 10 to 40 MeV. This would correspond to an increase of the E2 strength, since a_1 and a_3 are dominated by the E1-E2 interference as discussed before.

A suspicion for a possible failure of the low-energy calculations of the odd Legendre coefficients has recently been raised in an experiment by Stephenson et al. [45] who measured cross section ratios at different neutron laboratory angles with respect to 90° with a high accuracy. This experiment results in a significant deviation from the theoretical predictions below 8 MeV as shown in Fig. 11. We would like to mention that the experiment was repeated by Birenbaum et al. [46] but with considerably larger error bars and it is thus less conclusive. Since at the angles, where the ratios have been measured, the cross section varies rapidly, it serves as a microscope for the finer details of the differential cross section. To illustrate that point, the E2 strength has been increased artificially by 50 percent, which yields only a slight change in the cross section shape—a small shift to smaller angles—as shown in Fig. 12 at 5 MeV. But the corresponding cross section ratios in Fig. 11 change drastically.

Based on that experiment, there have been speculations by Hadjimichael et al. [47] that the E2 strength of the standard theory fails. By ad-hoc fitting the corresponding coefficients of the de Swart-Partovi parametrization of the cross section, they effectively increased the E2 strength and obtained a good agreement with the data.

As an example we show in Fig. 13 the coefficients a_1 through a_3 as extracted from the Stephenson data. But unfortunately, there are no other accurate measurements for a_1 in the critical energy range. Since a_0 has to be unchanged, it is again evident from the previous multipole analysis that only E1-E2 interferences could account for the deviations.

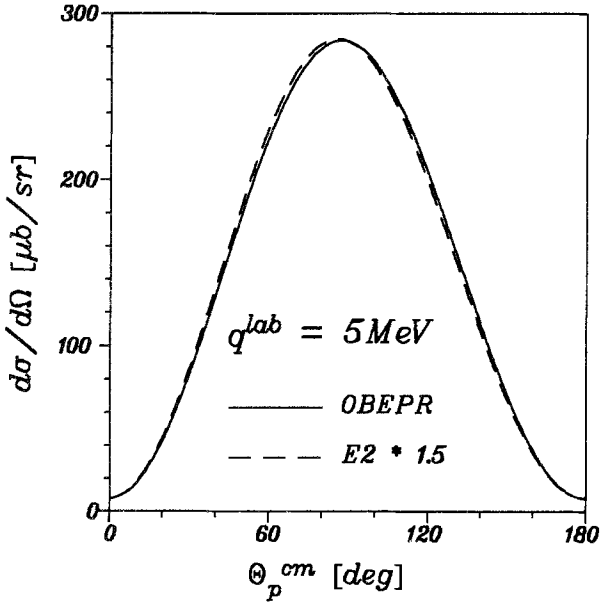

Fig. 12. Differential cross section at 5 MeV for the OBEPR and with the E2 strength artificially increased by 50 percent

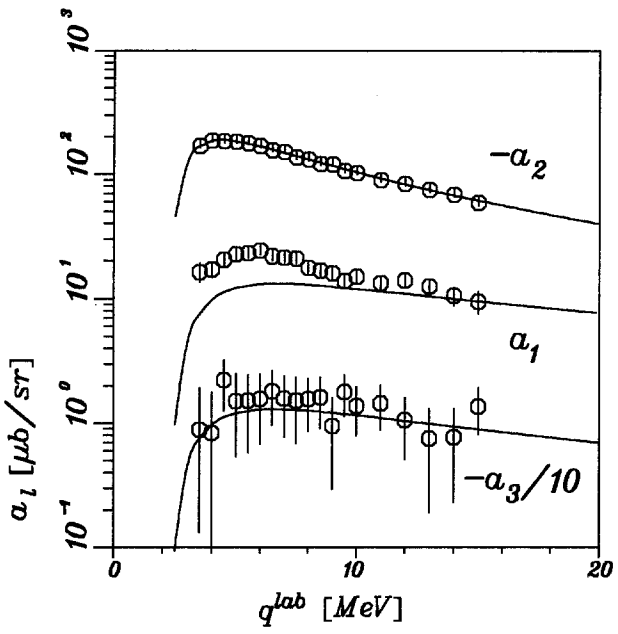

Fig. 13. The coefficients a_1–a_3 extracted from the data of ref. [45] in comparison with the OBEPQ predictions

Concerning the cross section ratios of Fig. 11, we would like to emphasize that the calculations are rather independent of the potential model and of any interaction current contributions beyond the normal part as well. Thus, they agree essentially with the Partovi calculation presented in ref. [45]. Since E2 enters dominantly via E1-E2 interferences, one might suspect as a possible theoretical error the phases of the E1 and E2 multipole matrix elements, which are determined by the *N-N* scattering phase shifts according to Watson's final-state theorem. But a careful analysis did not produce any sufficient cross section shift by artificially changing the phases within the experimental uncertainties. Furthermore, as discussed before, the dominant contributions to the E2 strength stem from isoscalar transitions which are mainly fixed by the nonrelativistic one-body convection current. This means that the effective increase of the E2 contribution would need an order of magnitude increase of the non-normal contribution by explicit iso-scalar exchange currents beyond the Siegert operator. On the other hand any such exchange current will be short-ranged and thus highly suppressed in the E2 operator. But if isoscalar exchange currents beyond the Siegert operators could play a role at all one would first expect their effect in isoscalar E1 transitions. They would then affect the a_1 coefficient via E1-M1 interference. Since this E1 transition is so small in the conventional calculation, one would need again a relatively huge exchange contribution not given by present exchange-current models. Thus, there seems to be no freedom at all in the standard calculations to produce such a change in the cross section shape. On the other hand, this shift of the angular distribution is so small that one should wait for an experimental confirmation before drawing definite conclusions concerning a failure of the conventional theory.

At very low energy, i.e. at 2.75 MeV, Smit and Brooks [48] recently remeasured the M1-E1 cross section ratio $\tau = \sigma_{M1}/\sigma_{E1}$. This ratio is given by $\tau = 3a/2b$ assuming an $(a + b \sin^2 \Theta_p^{cm})$-shape of the cross section, that is valid if only E1 and M1 are

Table 4. Dipole cross-section ratios $\tau = \sigma_{M1}/\sigma_{E1}$

		OBEP			
	Ref. [48] exp	-Q	-T	-R	Paris
τ	0.290 ± 0.021	0.271	0.264	0.275	0.275

present and if E1-M1 interference can be neglected. This assumption can be tested by evaluating

$$\Delta = \frac{\int d\cos\Theta_p^{cm} \left| \frac{d\sigma}{d\Omega} - (a + b \sin^2 \Theta_p^{cm}) \right|}{\int d\cos\Theta_p^{cm} \frac{d\sigma}{d\Omega}}, \tag{8}$$

where $d\sigma/d\Omega$ denotes the theoretical cross section, and a and b are calculated from Eq. (7). In fact, one obtains $\Delta \simeq 1.5$ percent at $q^{lab} = 2.75$ MeV. Furthermore, the coefficients a and b are given by M1-M1 and E1-E1 contributions, respectively, with only about 0.5 percent (0.05 percent) admixture of E1-E1 (M1-M1) contributions. The theoretical results for the dipole cross section ratio as listed in Table 4 are in acceptable agreement with this experiment.

Finally we consider the differential cross section at forward and backward angles, which plays an important role, since relativistic effects like the spin-orbit current manifest themselves here already at rather low energies.

In Fig. 14 we first show the multipole contributions to the forward and backward cross section. At energies below the minimum, which appears more distinct at forward direction, M1 is the dominant contribution. Then, with increasing energy, multipoles up to E2 and M2 become important on the few percent scale [49]. In particular, accurate measurements in the minimum region can provide information on the subtle interplay between E1 and M1 contributions.

Next we consider in Fig. 15 the various current contributions to the forward and backward cross section. In the energy region above 30 MeV, the major contribution beyond the normal part is quite distinctly the spin-orbit current, as it was first pointed out by Cambi et al. [13]. It decreases the cross section by about 15 percent at 40 MeV. However, at lower energies, especially in the minimum region, the explicit MEC corrections to the normal part become more important.

Concerning the experimental data on forward and backward cross sections (see Fig. 16) one faces a rather open situation. Whereas the data fit quite well the theoretical predictions in the minimum region, some inconsistencies seem to exist at higher energies. In forward direction the data support a still smaller cross section than the theory at energies above 30 MeV. At backward angles, for instance, the data of refs. [42] and [54] are obviously incompatible with each other. On the other hand, the forward-backward asymmetry is described quite well, except for the data of ref. [54], which lies too low at 0° and too high at 180°. Despite a lot of recent experimental efforts, one cannot be satisfied with the present experimental data being still not conclusive.

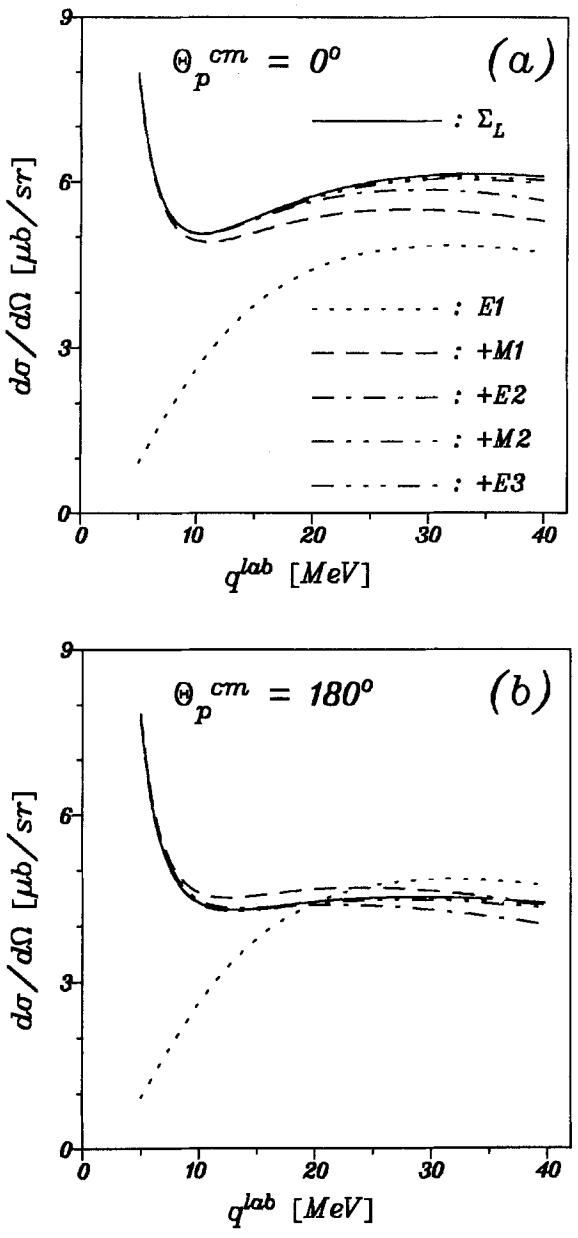

Fig. 14. Electromagnetic multipole contributions to the forward and backward cross section for the OBEPR. The notation for the interfering multipoles is the same as in Fig. 4

5 Polarization Observables

Besides the fact that the unpolarized cross section as considered so far still deserves further efforts especially concerning more accurate measurements, the experimental emphasis will certainly shift towards polarization observables in the future. On the theoretical side, all pieces for the interpretation of the most general polarization measurements on deuteron photodisintegration are available at present. Therefore it should be a real challenge to look beyond single-polarization observables. From the theoretical point of view, there is strong support for such experiments. Unpolarized experiments give only limited, i.e., averaged information as contained in the reaction T-matrix. Thus any sufficiently accurate polarization measurement will

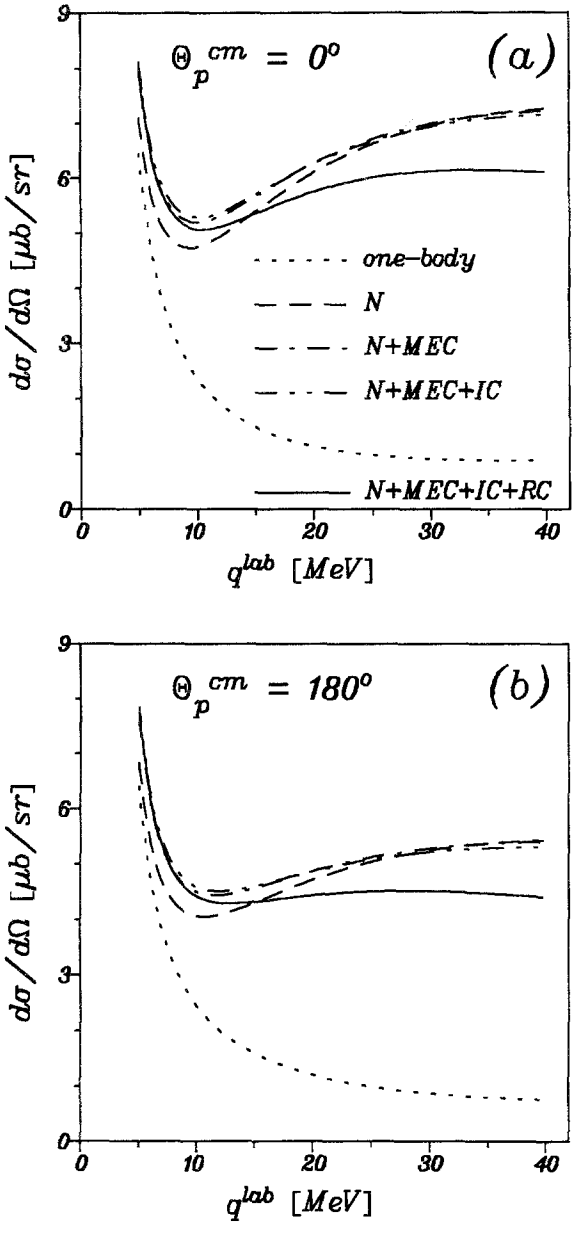

Fig. 15. The composition of the forward and backward cross section for the OBEPR from the various electromagnetic current contributions

help to increase our understanding of this process and will allow to test in greater detail the validity of the underlying theoretical concepts. As is well known, 23 independent polarization measurements in conjunction with the unpolarized cross section provide the maximum possible knowledge of this process. Recently, such a set of experiments has been constructed explicitly [58]. A different approach has been pursued in ref. [59]. But since any such set always includes four-fold polarization experiments, a complete determination of the T-matrix is not yet feasible.

In the energy region below 40 MeV, up to now only the photon asymmetry Σ^l and the neutron polarization $P_y(n)$ along the y-axis, which is perpendicular to the reaction plane, have been measured. The angular distribution of Σ^l is in rather good agreement with the theoretical predictions (see Figs. 17 a–c). Obviously, there is

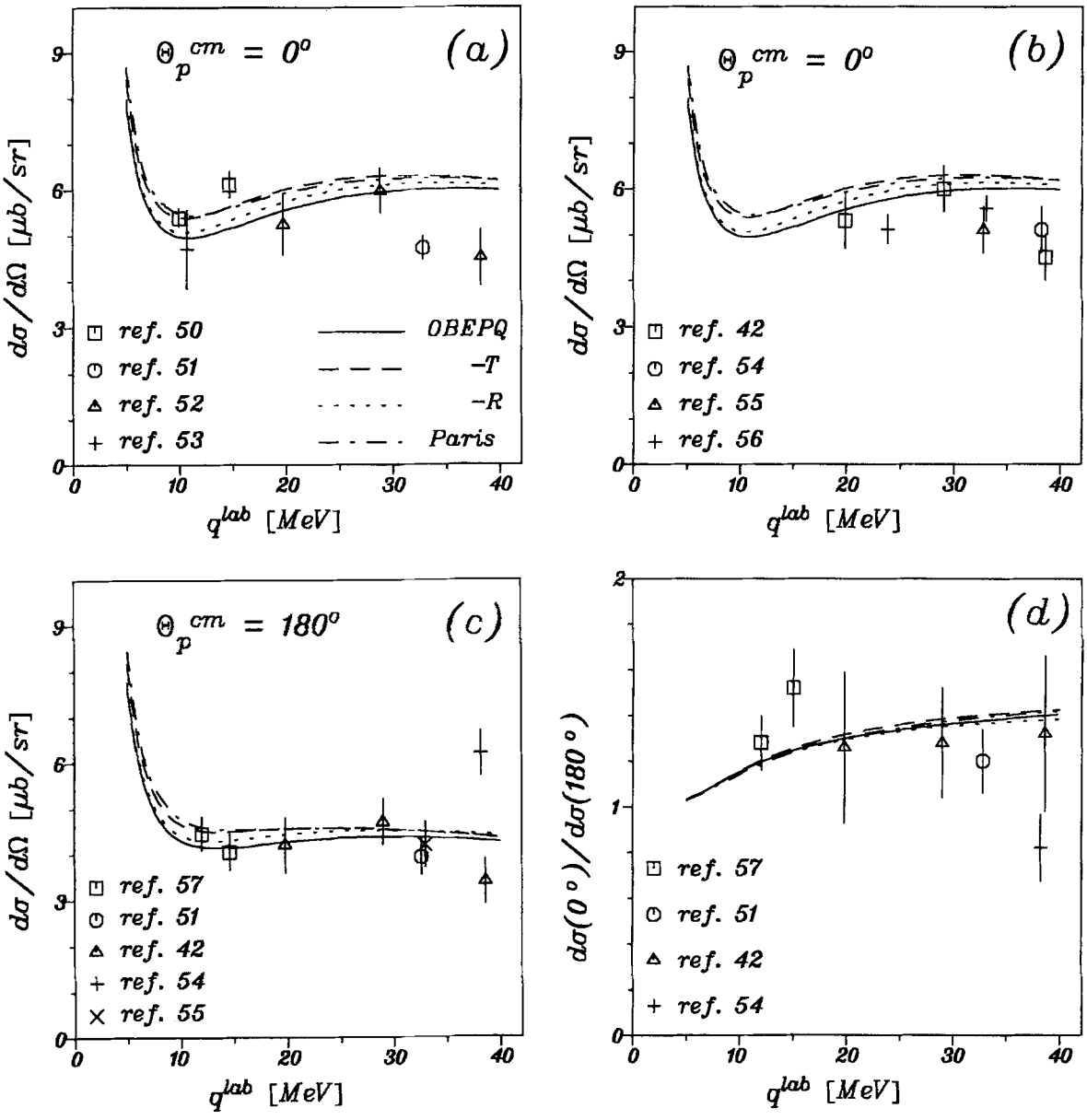

Fig. 16. Comparison of the experimental forward (a, b) and backward (c) cross section and of the forward-backward asymmetry (d) with the theoretical predictions

almost no potential-model dependence of the photon asymmetry at these energies. Furthermore, all contributions beyond the normal part are negligibly small. But the experimental resolution is high enough to rule out a calculation ignoring MEC. The energy dependence of Σ^l at $\Theta_p^{cm} = 90°$ is shown in Fig. 17 d. Again, the data are in good agreement with the calculations.

Fig. 18 a shows the angular distribution of $P_y(n)$ at $q^{lab} = 2.75$ MeV. At this low energy $P_y(n)$ turns out to be very insensitive to effects from MEC, IC, and RC. Even if the dependence of $P_y(n)$ on the potential model is more pronounced than for Σ^l, the possible variations seem not to be able to account for the deviation from

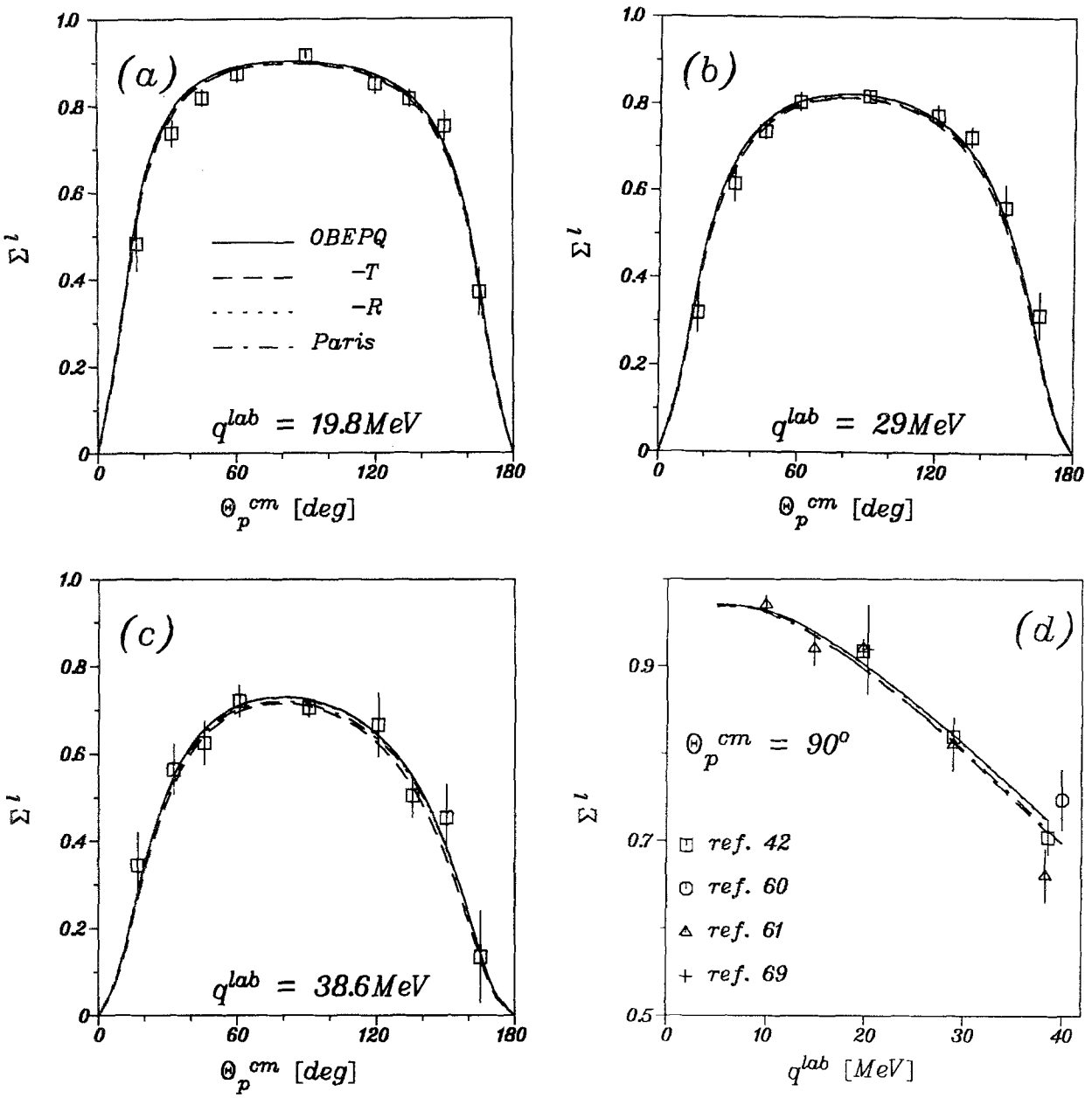

Fig. 17. The photon asymmetry Σ^l compared to theoretical predictions: (a)–(c) angular dependence at different energies, (d) energy dependence at 90°

experiment (see also ref. [62]). But as already mentioned in ref. [63], an additional systematic error due to calibration problems of the neutron polarimeter cannot be excluded. Therefore, it would be desirable to have some new data on $P_y(n)$ at this low energy.

Finally, the energy dependence of $P_y(n)$ at fixed neutron angles is considered in Figs. 18 b–d. In (b) and (c) the calculations refer to $\Theta_n^{cm} = 90°$, whereas the experimental angles differ slightly from this value, referring partially to $\Theta_n^{lab} = 90°$, for the photodisintegration process or to $\Theta_q^{cap} = 90°$, the latter being the lab angle between

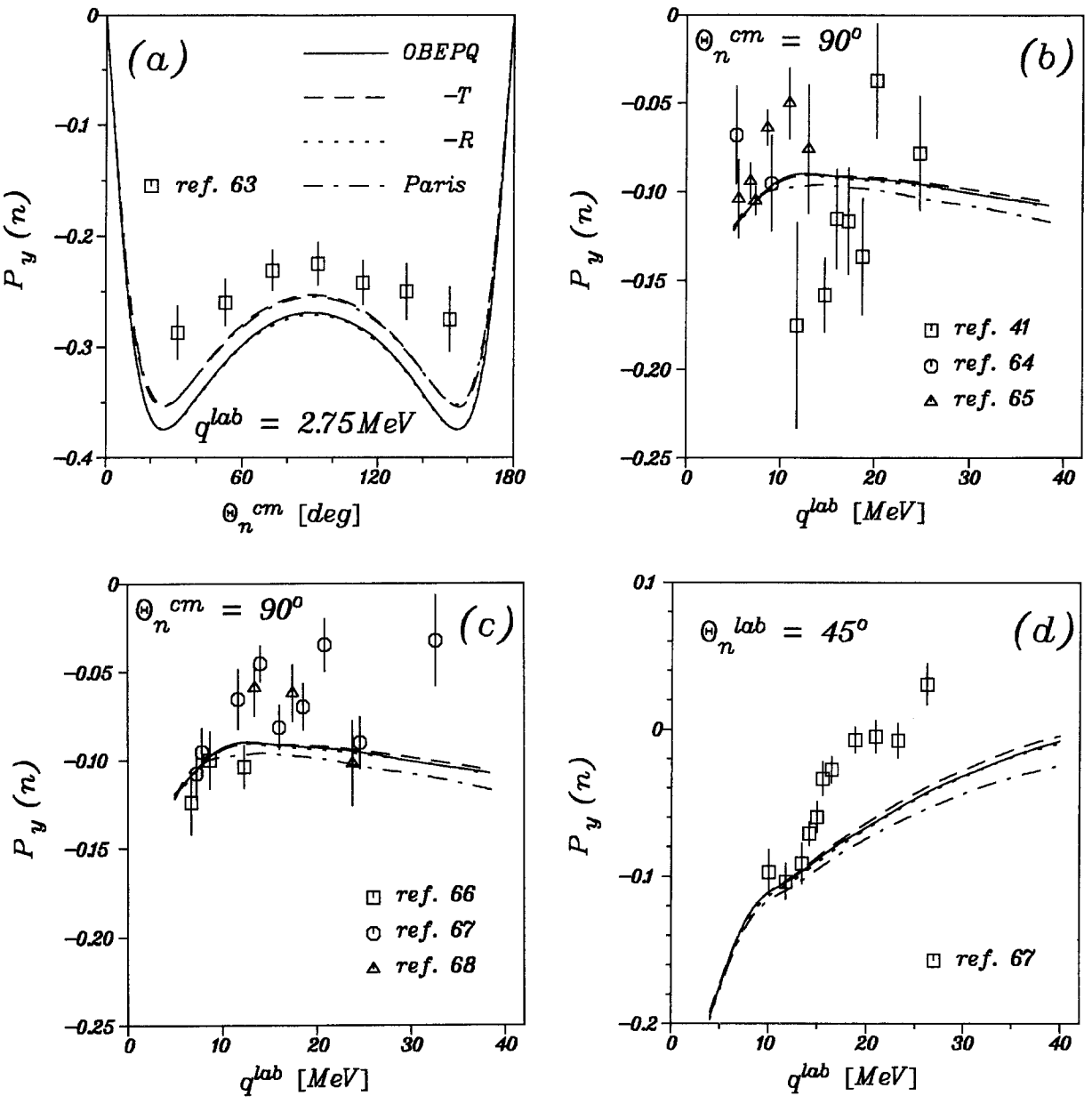

Fig. 18. Comparison of neutron polarization data on $P_y(n)$ with theoretical results as $q^{lab} = 2.75$ MeV (a), and energy dependence of $P_y(n)$ at neutron angles $\Theta_n^{cm} = 90°$ (b, c) and $\Theta_n^{lab} = 45°$ (d)

the incident neutron and the outgoing photon in the inverse capture reaction. However, since the angular distribution of $P_y(n)$ is rather flat at 90°, this difference is negligible compared to the statistical uncertainties. Facing the broad range of results from different experiments at 90° in comparison to the narrow band of theoretical calculations it is difficult to draw conclusions. In ref. [64] it was stated that leaving out the data of ref. [66] all experiments of that time were mutually consistent, resulting in a significantly less negative $P_y(n)$ than theoretically predicted. This fact was then interpreted as an indication for some missing ingredient in the

theory. However, the recent data of ref. [41] is at variance with this conclusion in showing a larger negative neutron polarization.

In Fig. 18 d calculations and data refer to $\Theta_n^{lab} = 45°$. The data of ref. [67] indicate an energy dependence of $P_y(n)$ significantly different to the calculations. However, here the situation may be similar to that at 90°, so that further independent measurements are required.

6 Summary

In the preceeding sections we have tried to collect all existing experimental data on deuteron photodisintegration in the energy region from threshold up to 40 MeV, even though it is likely that we have missed some. These data have been compared to theoretical predictions in the framework of conventional nonrelativistic calculations including consistently meson-exchange currents. In addition, isobar configurations and relativistic corrections, most prominently the spin-orbit current, have been taken into account. As N-N potentials we have used either the Paris potential or OBE approximations to the Bonn potential. Comparison was made for the unpolarized total and differential cross section, the photon asymmetry Σ^l and the neutron polarization $P_y(n)$.

Over the years, the largest experimental effort was dedicated to the total cross section. Apart from some experiments, which obviously contradict the general trend, the large data base could be used in principle to exclude certain models by statistical arguments. However, such a procedure is not perfectly conclusive, since unknown systematic errors are most likely to be present. In order to differentiate between the predictions of different models, an accuracy of less than 5 percent (at 40 MeV, say) is required. Thus, new high-precision measurements of the total cross section are still a matter of interest.

The situation for the differential cross section is much less homogeneous. Definite angular distributions have been measured with rather good statistical accuracy, which, however, is still not high enough in order to allow to differentiate between different theoretical models. Furthermore, it has to be noted that different measurements at the same energy involve mutual incompatibilities. This is obviously true also for the forward cross section, which necessarily has to be measured more precisely in the energy region considered here. Concerning the experiment of ref. [45] on very accurate cross-section ratios, we believe that it is too early to draw the definite conclusion that new theoretical ingredients are needed unless the results are independently confirmed.

Measurements of polarization observables are the real challenge for the future. This is because they are in general very sensitive to the underlying theoretical model. But up to now, the available data are neither of good enough quality, nor free of inconsistencies. While the sophistication of future polarization measurements will certainly increase, we think that it is also very important not to neglect efforts to determine the simpler observables, as for example the unpolarized differential cross section, with considerably higher accuracy.

References

1. Arenhövel, H., Sanzone, M.: Photodisintegration of the Deuteron: A Review of Theory and Experiment (Few-Body Systems, Suppl. 3). Wien-New York: Springer 1991

2. Chadwick, J., Goldhaber, M.: Nature **134**, 237 (1934)
3. Machleidt, R., Holinde, K., Elster, C.: Phys. Rep. **149**, 1 (1987)
4. Lacombe, M., et al.: Phys. Rev. **C21**, 861 (1980)
5. Desplanques, B.: Phys. Lett. **B203**, 200 (1988)
6. Machleidt, R.: Adv. Nucl. Phys. **19**, 189 (1989)
7. Leidemann, W., Schmitt, K.-M., Arenhövel, H.: Phys. Rev. **C42**, 826 (1990)
8. Schmitt, K.-M., et al.: Phys. Rev. **C41**, 841 (1990)
9. Schmitt, K.-M., Arenhövel, H.: Few-Body Systems **7**, 95 (1989)
10. Schmitt, K.-M., Arenhövel, H.: Few-Body Systems **6**, 117 (1989)
11. Fabian, W., Arenhövel, H.: Nucl. Phys. **A314**, 253 (1970); Leidemann, W.: Private Communication (1988)
12. Wilhelm, P., Leidemann, W., Arenhövel, H.: Few-Body Systems **3**, 111 (1988)
13. Cambi, A., Mosconi, B., Ricci, P.: Phys. Rev. Lett. **48**, 462 (1982)
14. Bethe, H. A., Longmire, C.: Phys. Rev. **77**, 647 (1950)
15. Wauters, P., et al.: Few-Body Systems **8**, 1 (1990)
16. Moreh, R., Kennett, T. J., Prestwich, W. V.: Phys. Rev. **C39**, 1247 (1989)
17. Bernabei, R., et al.: Phys. Rev. Lett. **57**, 1542 (1986)
18. Birenbaum, Y., Kahane, S., Moreh, R.: Phys. Rev. **C32**, 1825 (1985)
19. Stiehler, T., et al.: Phys. Lett. **151B**, 185 (1985)
20. De Pascale, M. P., et al.: Phys. Lett. **119B**, 30 (1982)
21. Bosman, M., et al.: Phys. Lett. **82B**, 212 (1979)
22. Ahrens, J., et al.: Phys. Lett. **52B**, 49 (1974)
23. Skopik, D. M., Shin, Y. M., Phenneger, M. C., Murphy, J. J.: Phys. Rev. **C9**, 531 (1974)
24. Baglin, J. E. E., Carr, R. W., Bentz, E. J., Wu, C.-P.: Nucl. Phys. **A201**, 593 (1973)
25. Mafra, O. Y., Kuniyoshi, S., Goldemberg, J.: Nucl. Phys. **A186**, 110 (1972)
26. Weissman, B., Schultz, H. L.: Nucl. Phys. **A174**, 129 (1971)
27. Tudorić-Ghemo, J.: Nucl. Phys. **A92**, 233 (1967)
28. Cerineo, M., Ilakovac, K., Šlaus, I., Tomaš, P.: Phys. Rev. **124**, 1947 (1961)
29. Whetstone, A., Halpern, J.: Phys. Rev. **109**, 2072 (1958)
30. Allen, L.: Phys. Rev. **98**, 705 (1955)
31. McMurray, W. R., Collie, C. H.: Proc. Phys. Soc. **68A**, 181 (1955)
32. Marin, P., Bishop, G. R., Halban, H.: Proc. Phys. Soc. **67A**, 1113 (1954)
33. Barnes, C. A., Carver, J. H., Stafford, G. H., Wilkinson, D. H.: Phys. Rev. **86**, 359 (1952); Carver, J. H., Wilkinson, D. H.: Nature **167**, 154 (1951)
34. Wäffler, H., Younis, S.: Helv. Phys. Acta **24**, 1947 (1951)
35. Bishop, G. R., et al.: Phys. Rev. **80**, 211 (1950)
36. Hough, P. V. C.: Phys. Rev. **80**, 1069 (1950)
37. Phillips, J. A., Lawson, Jr., J. S., Kruger, P. G.: Phys. Rev. **80**, 326 (1950)
38. Snell, A. H., Barker, E. C., Sternberg, R. L.: Phys. Rev. **80**, 637 (1950)
39. de Swart, J. J.: Physica **25**, 233 (1959)
40. Partovi, F.: Ann. Phys. (NY) **27**, 79 (1964)
41. Fink, G., et al.: Preprint KFK (1989)
42. De Pascale, M. P., et al.: Phys. Rev. **C32**, 1830 (1985)
43. Rossi, P., et al.: Phys. Rev. **C40**, 2412 (1989)
44. Thorlacius, A. E., Fearing, H. W.: Phys. Rev. **C33**, 1830 (1986)
45. Stephenson, K. E., Holt, R. J., McKeown, R. D., Specht, J. R.: Phys. Rev. **C35**, 2023 (1987)
46. Birenbaum, Y., et al.: Phys. Rev. Lett. **61**, 810 (1988)
47. Hadjimichael, E., Rustgi, M. L., Pandey, L. N.: Phys. Rev. **C36**, 44 (1987)
48. Smit, F. D., Brooks, F. D.: Nucl. Phys. **A465**, 429 (1987)
49. Friar, J. L., Gibson, B. F., Payne, G. L.: Phys. Rev. **C30**, 441 (1984)
50. De Graeve, A., et al.: Phys. Lett. **B227**, 321 (1989)

51. Ninane, A., et al.: Phys. Rev. **C35**, 402 (1987)
52. Matone, G., et al.: Proc. Int. School of Intermediate-Energy Nuclear Physics, Verona (Bergère, R., Costa, S., Schaerf C., eds.), p. 505. Singapore: World Scientific 1986
53. Zieger, A., Grewer, P., Ziegler, B.: Few-Body Systems **1**, 135 (1986)
54. Dupont, C., et al.: Nucl. Phys. **A445**, 13 (1985); Gilot, J. F., et al.: Phys. Rev. Lett. **47**, 304 (1981)
55. Ninane, A., et al.: Can. J. Phys. **62**, 1104 (1984)
56. Hughes, R. J., Zieger, A., Wäffler, H., Ziegler, B.: Nucl. Phys. **A267**, 329 (1976)
57. De Graeve, A.: Doctoral Thesis. Gent: 1988
58. Arenhövel, H., Schmitt, K.-M.: Few-Body Systems **8**, 77 (1990)
59. Dmitrasinovic, V., Gross, F.: Phys. Rev. **C40**, 2479 (1989)
60. Barannik, V. P., et al.: Yad. Fiz. **38**, 1108 (1983); Sov. J. Nucl. Phys. **38**, 667 (1983)
61. Del Bianco, W., et al.: Phys. Rev. Lett. **47**, 1118 (1981)
62. Rustgi, M. L., Vyas, R., Chopra, M.: Phys. Rev. Lett. **50**, 236 (1983)
63. Jewell, R. W., John, W., Sherwood, J. E., White, D. H.: Phys. Rev. **139**, B71 (1965)
64. Soderstrum, J. P., Knutson, L. D.: Phys. Rev. **C35**, 1246 (1987)
65. Holt, R. J., Stephenson, K. E., Specht, J. R.: Phys. Rev. Lett. **50**, 577 (1983)
66. Drooks, L. J.: Ph.D. Thesis. Yale University 1976
67. Nath, R., Firk, F. W. K., Schultz, H. L.: Nucl. Phys. **A194**, 49 (1972)
68. Bertozzi, W., et al.: Phys. Rev. Lett. **10**, 106 (1963)
69. Del Bianco, W., et al.: Nucl. Phys. **A343**, 121 (1980)
70. Michel, P., et al.: J. Phys. **G15**, 1025 (1989)
71. Arenhövel, H.: Few-Body Systems **4**, 55 (1988)
72. Cambi, A., Mosconi, B., Ricci, P.: Phys. Rev. **C26**, 2358 (1982)

Received December 3, 1990; accepted for publication February 14, 1991